The Influence of Synthesis Conditions on The Electrorheological Performance of Iron(II) Oxalate Rod-like Particles

Erika Kutalkova[1], Alena Ronzova[1,2], Josef Osicka[1], David Skoda[1], Michal Sedlacik[1,2,*]

[1]Centre of Polymer Systems, University Institute, Tomas Bata University in Zlín, Trida T. Bati 5678, 760 01 Zlín, Czech Republic

[2]Department of Production Engineering, Faculty of Technology, Tomas Bata University in Zlín, Vavrečkova 275, 760 01 Zlín, Czech Republic

[*]corresponding author: msedlacik@utb.cz

Abstract

This study investigates the influence of synthesis conditions of iron(II) oxalate particles on the particle morphology for their utilization in smart materials known as electrorheological (ER) fluids. Particle morphology has a significant impact on the ER behavior of the particles enabling their use in many unique practical applications. In this study, fifteen various iron(II) oxalate particles differing in synthesis conditions were prepared, out of which four variations were selected for an in depth investigation due to their promising morphology. The influence of synthesis conditions on the morphology of the resulted particles was evaluated by scanning electron microscopy analysis. An X-ray diffraction analysis was employed to confirm the dominant $FeC_2O_4 \cdot H_2O$ phase presented in the synthesized particles. The ER suspensions consisted of the selected four iron(II) oxalate particles dispersed in silicone oil. An optical microscope and a rheometer, both operating under external electric field, enabled a precise and accurate investigation of the structure, the ER performance. Visual observation was used to evaluate the sedimentation stability of the suspension.

Keywords: electrorheology, iron oxalate particles, morphology, rod-like particles, synthesis conditions, sedimentation

1. Introduction

Electrorheological (ER) fluids are classified as smart systems whose rheological properties, such as viscosity, yield stress etc., can be tuned using an external electrical field [1, 2]. These systems can shift from a liquid to a solid-like state in a very short time of milliseconds [3]. Thus, ER fluids are potential candidates in various engineering areas such as damping systems [4, 5], actuators [6, 7], robotics [8], tactile display [9-11], and torque elements for use in rehabilitation devices [12, 13]. Electrorheological fluids typically consist of electrically polarizable particles well-dispersed in non-conducting liquid medium [1, 14]. These particles are randomly spread in the liquid under normal conditions, however, with the application of an external electrical field, organized chain-like structures are formed. As a result, the viscoelastic and mechanical properties are enhanced rapidly [15]. Typically, the apparent viscosity and viscoelastic moduli are increased by several orders of magnitude due to the presence of the electric field, this increasement is commonly known as the ER effect. The intensity of the ER effect is depended on many parameters, such as the strength of the electric field applied, volume fraction [16], and properties of the particles, such as size, morphology [2, 17], and conductivity [18]. Furthermore, the ER effect heavily depends on dielectric permittivity of the particles, relaxation time and dielectric relaxation strength of the ER fluid as well as the temperature of the system. Hence, these parameters significantly influence the transition from liquid to solid-like state [14, 19].

Intensive research has been conducted to develop high-performance ER particles to enable a practical application of ER suspensions and for that reason the origins of the ER effect are of a great importance. Due to the formation of these chain-like structures the distance between these particles is very short, thus the ER effect is connected to the polarization of dispersed particles and the interaction between them when an external electric field is applied. At rest; the particle shape is expected to regulate the field-induced structure and the aggregate break-up, friction,

and dissipation mechanisms under shear [20, 21]. The yield stress (τ_y) represents one of the key parameters of ER fluids and is defined as the stress which the ER fluids withstand before they start flowing. However, from a practical point of view, it is necessary to develop ER material with high τ_y as well as low field-off viscosity and favorable sedimentation stability [22]. The morphology and the size of the particles also play a crucial role for an enhanced ER performance. Previous research groups have demonstrated that one-dimensional materials, particularly represented by rod-like particles, exhibits a higher ER effect and efficiency compared to spherical ones. This benefit arises from the high aspect ratio (L/D) of the rods [23, 24]. Under an external electric field, the particles are oriented with their longer axis in this field's direction. Friction forces, in addition to dipole-dipole interactions created among the particles, are considerably stronger resulting in more robust and rigid chain-like structure [25]. In the case of one-dimensional particles, the ER effect can be sufficiently enhanced even for low volume fractions. Additionally, the rod-like particles has proved an ability to suppress sedimentation in comparison to the spherical ones due to the limited rotational motion in the carrier medium [26]. As reported previously [27], rod-like ER fluids show enhanced dielectric properties with increasing aspect ratios. Unfortunately, undesirable high field-off viscosity due to their higher viscous drag forces are observed [28].

The works done before were focused on the preparation of one-dimensional particles appropriate for ER fluids by hydrothermal techniques under alkali conditions [29], nevertheless these approaches can be dangerous due to the use of high temperatures and pressure, not to mention that the time of the synthesis is rather long. One of the other methods of synthesizing a shaped anisotropic material with exceptional properties is a molten salt co-precipitation technique. This simple method may produce a single-phase multicomponent oxides, mostly using the molten salt as a reaction medium [30-32]. The reaction time of this procedure is shorter enabling the growth of crystals in a specific direction. Varying the precursor's molar

ratio and the co-precipitation setting, it is possible to prepare particles with different morphology, size, high-purity and stoichiometrically-optimized [33] which generate desirable ER effects. Lastly, this method is cheap, thus enabling large-scale production [34].

This work focuses on the synthesis of iron(II) oxalate dihydrate ($FeC_2O_4 \cdot 2H_2O$) particles by means of a co-precipitation method. The controlled variation in reaction conditions led to the preparation of-particles with different sizes and morphologies, aiming to optimize the particles' preparation to achieve the highest ER effect possible. In addition, the particles synthetized by this one-step method exhibit improved ER performance in comparison to the recently published ER materials [35]. The iron(II) oxalate particles possessing rod-like morphology appear to be suitable for practical applications in electrorheology.

2. Materials and Methods

2.1. Materials

The preparation of the particles included iron(II) sulphate heptahydrate ($FeSO_4 \cdot 7H_2O$, ≥ 99%, Sigma Aldrich, USA) was used as a source of Fe^{2+} ions in addition to oxalic acid dihydrate ($C_2H_2O_4 \cdot 2H_2O$, p.a., Lach-Ner, Czech Republic) and ethylene glycol (Penta, Czech Republic). Silicone oil (Lukosiol M200, Chemical Works Kolín, Czech Republic, viscosity η = 194 mPa·s, conductivity $\sigma \approx 10-11$ S·cm^{-1}) was used as the dispersed phase.

2.2. Synthesizing the Particles

The iron(II) sulphate heptahydrate was used as a source of Fe^{2+} ions and oxalic acid dihydrate was utilized as a precipitating agent for the preparation of the iron (II) oxalate particles. The impact of the conditions under which the iron(II) oxalate particles were synthesized was investigated, highlighting the effect of morphology. The prepared mixtures were formed from 20 mmol of $FeSO_4 \cdot 7H_2O$ or $C_2H_2O_4 \cdot 2H_2O$ dissolved in a mixture of ethylene glycol and

demineralized water at ratio of 3:1, in volume 28 mL. Immediately after, the dissolved $C_2H_2O_4 \cdot 2H_2O$ was added to a solution of $FeSO_4 \cdot 7H_2O$ using various drip rates and stirring rates. Finally, the mixture was left in mechanical stirring conditions for a defined time as can be seen in Table 1.

Table 1: Variation in the synthesis conditions for the iron(II) oxalate particles.

	Labeling	Drip rate [mL/h]	Stirring rate [rpm]	Stirring time [hrs]
1	OX5	14	100	12
2	OX6	2.3	100	12
3	OX7	1.16	100	12
4	OX8	14	1000	12
5	OX9	2.3	1000	12
6	OX10	1.16	1000	12
7	OX11	14	100	2
8	**OX1**	**2.3**	**100**	**2**
9	**OX3**	**1.16**	**100**	**2**
10	OX12	14	1000	2
11	OX13	2.3	1000	2
12	OX14	1.16	1000	2
13	OX15	14	500	2
14	**OX2**	**2.3**	**500**	**2**
15	**OX4**	**1.16**	**500**	**2**

Considering the results of a previous study [36], in which it was observed that the drip rate affected the morphology of the resulting particles, a variety of drip rate values was applied. The

precise drip rate was achieved by programmable syringe pump NE-1000 (KF Technology, Italy). Thus, three variable parameters of the synthesis have been defined. Finally, a formed yellow precipitate was thoroughly filtered-off and washed with distilled water several times. The washed and filtered yellow precipitate was dried for 12 hours under 10 mbar at 70 °C.

2.3. The Characterization of the Particles

The morphology of the prepared particles was investigated using a scanning electron microscopy – Phenom Pro (SEM, Phenom-World, the Netherlands) operated at 10 kV. The length and the width of the prepared rod-like particles were analyzed using software Image J 1.52a. It is worth mentioning that the duration of stirring does not influence the samples shape and size. After evaluating the SEM images, four types of prepared iron(II) oxalate particles differing in morphology were further used for investigation. The description of synthesis parameters and coding of the iron(II) oxalate particles used in this study is presented in Table 2 (Table S1 refers to all of the prepared samples/variants). The reproducibility of the synthesis process of the particles was verified-with three independent repetitions.

Table 2: Synthesis conditions for the iron(II) oxalate particles and their dimensional characteristics.

Drip rate [mL/h]	**Stirring rate** [rpm]	**Stirring time** [hrs]	**Code**	***L*** [µm]	***D*** [µm]	***L/D*** [–]
2.30	100	2	OX1	0.90±0.26	0.17±0.04	5.29
2.30	500	2	OX2	2.20±0.89	0.33±0.08	6.67
1.16	100	2	OX3	1.24±0.30	0.16±0.04	7.75
1.16	500	2	OX4	2.24±0.82	0.43±0.10	5.21

The density was measured using a gas pycnometer (UltraFoam 1200e, Quantachrome Instruments, Germany) operating with a nitrogen medium. The densities of the particles were calculated from ten independent measurements and are listed in Table 3.

For the evaluation of the crystalline structure and the phase composition of the iron(II) oxalate particles, X-ray diffractometry was performed using a Rigaku MiniFlex 600 equipped with a $Co_{K\alpha}$ (λ = 1.7903 Å) X-ray tube (40 kV, 15 mA). Data processing and crystal size calculations were investigated with Rigaku PDXL2 software. The average crystalline size of the crystallites was evaluated using the Scherrer's formula, $d = K\lambda/\beta\cos\theta$, where d is the crystallite size, K is a grain shape dependent constant (0.94), λ is the wavelength, θ is a Bragg reflection angle and β is the full-width half-maximum. The observed line broadening was corrected to intrinsic sample broadening using an instrumental function using B-spline background subtraction and a Split pseudo-Voigt peak shape function.

The conductivity of the synthesized iron(II) oxalate particles (results in Table 3) was measured using a two-point method at room temperature by means of an electrometer (Keithley 6517B, USA).

2.4.The Preparation of Electrorheological Suspensions

The suspensions for the ER measurement were prepared by mixing the synthesized iron(II) oxalate particles with a silicone oil in two concentrations, 5 vol% and 10 vol%. The ER suspensions were stirred using a glass stick for 5 minutes before each measurement. Immediately after, the samples were placed into an Ultrasonic processor (UP400S, Hielscher, Germany) for further homogenization by applying 25 seconds of ultrasonication at 30 % vibration amplitude after 0.4 cycles. This step was necessary to obtain a thorough homogenization of the ER suspension.

2.5.Optical Microscopy

The formation of internal chain-like structures created by the iron(II) oxalate particles dispersed in the ER suspensions in the presence of an external electric field was investigated by means of an optical microscopy. The ER suspension (0.5 vol%) was placed on a glass plate between two copper electrodes. An external electric field strength of 0.5 $kV \cdot mm^{-1}$ was supplied by a DC high-voltage source (Keithley 2400, USA). The resulting structures were observed using an optical microscope (Leica DVM2500; Leica Microsystems, UK).

2.6.Electrorheological Measurements

The ER measurements were performed under a controlled shear rate mode at shear rates of 0.1–150 s^{-1} using a Bohlin Gemini rotational rheometer (Malvern Instruments, UK) with a plate–plate geometry (20 mm in diameter with a gap of 1 mm). The ER behavior was investigated both, in the presence and absence of an external electric field. External electric field with values ranging between 0.3 and 1.5 $kV \cdot mm^{-1}$ was generated by a DC high-voltage source TREK 668B (TREK, USA). Before each measurement the suspension was exposed to an external electric field for 1 minute. The field was sufficient enough for the particles to be organized in chain-like structures during this time. After each measurement, the ER suspension was sheared for 1 minute at a constant shear rate of 20 s^{-1} without the presence of any electric field to recover the suspension to its initial state with the particles randomly dispersed throughout the carrier liquid.

3. Results and Discussion

3.1.The Characterization of the Particles

The morphology of the iron(II) oxalate particles was investigated using SEM with selected images of the particles enlisted in Table 2 shown in Fig. 1. The SEM images for the remaining particles of Table 1 not used in ER suspensions are presented in Fig. S1. Figures 1a,b show the

morphology of the iron(II) oxalate particles synthesized with a drip rate of $C_2H_2O_4{\cdot}2H_2O$ of 2.3 mL/h and different stirring rates. As presented in Fig. 1a, the OX1 particles which were stirred at 100 rpm during their synthesis have a rod-like morphology. These particles share similar lengths (L) with an average of L= 0.90±0.26 μm and comparable diameters (D) of D = 0.17±0.04 μm. Then a geometric aspect ratio can be extracted L/D = 5.3. On the other hand, the OX2 (Fig. 1b) particles, which were stirred at 500 rpm during the synthesis process, showed increased values of L = 2.20±0.89 μm while preserving the diameter D = 0.33±0.08 μm resulting in an aspect ratio of L/D = 6.7. Thus, it is evident that a higher stirring rate during the synthesis leads to more robust rod-like particles with a higher one-dimensional character. The higher the stirring rate of 500 rpm results in a faster growth of crystalline particles, which is a consequence of the dripping $C_2H_2O_4{\cdot}2H_2O$ being dispersed faster into $FeSO_4{\cdot}7H_2O$ leading to more frequent particles nucleation.

The effect of a lower drip rate is shown in Fig. 1c,d for particles synthesized using the same stirring rates. The OX3 particles prepared with a stirring rate of 100 rpm (Fig. 1c) show a quite uniform rod-like morphology with an average L = 1.24±0.30 μm and D = 0.16±0.04 μm resulting in L/D = 7.8. The last sample taken for investigation of its ER performance based on OX4 particles is shown in Fig. 1d. Similarly to OX2, increasing the stirring rate, results in a higher L (2.24±0.82 μm), while the D (0.43±0.10 μm) is not as different, altogether resulting in L/D = 5.2. In a similar way, this high stirring rate results in the formation of more robust iron(II) oxalate particles and despite using a lower drip rate, a higher rod-like character was noticed with a lower reaction mixture stirring probably enabling better particle nucleation.

The results above are summarized in Table 2 which gives a direct comparison between the dimensional characteristics of the iron(II) oxalate for various synthesis conditions. Evidently the aspect ratio seems to be independent of both drip and stirring rate. However, the particle's length varied significantly as longer particles are generally obtained with faster stirring of the

synthesis mixture, regardless of the drip rate. A similar trend can be observed for the diameter of rod-like particles. It can be concluded that the morphological characteristics of the particles can be tuned using different synthesis conditions. To be specific, by comparing the pairs with the same stirring and drip rates, it can be concluded that the dimensions of the particles are affected mostly by the stirring rate. The drip rate seems to have a much smaller impact on the dimensional characteristics of the particles. The OX2 and the OX4 samples possess almost the same length and diameter, which are almost twice as high in comparison with OX1 and OX2. In addition, OX3 has the highest aspect ratio which should have a positive effect on the ER behavior.

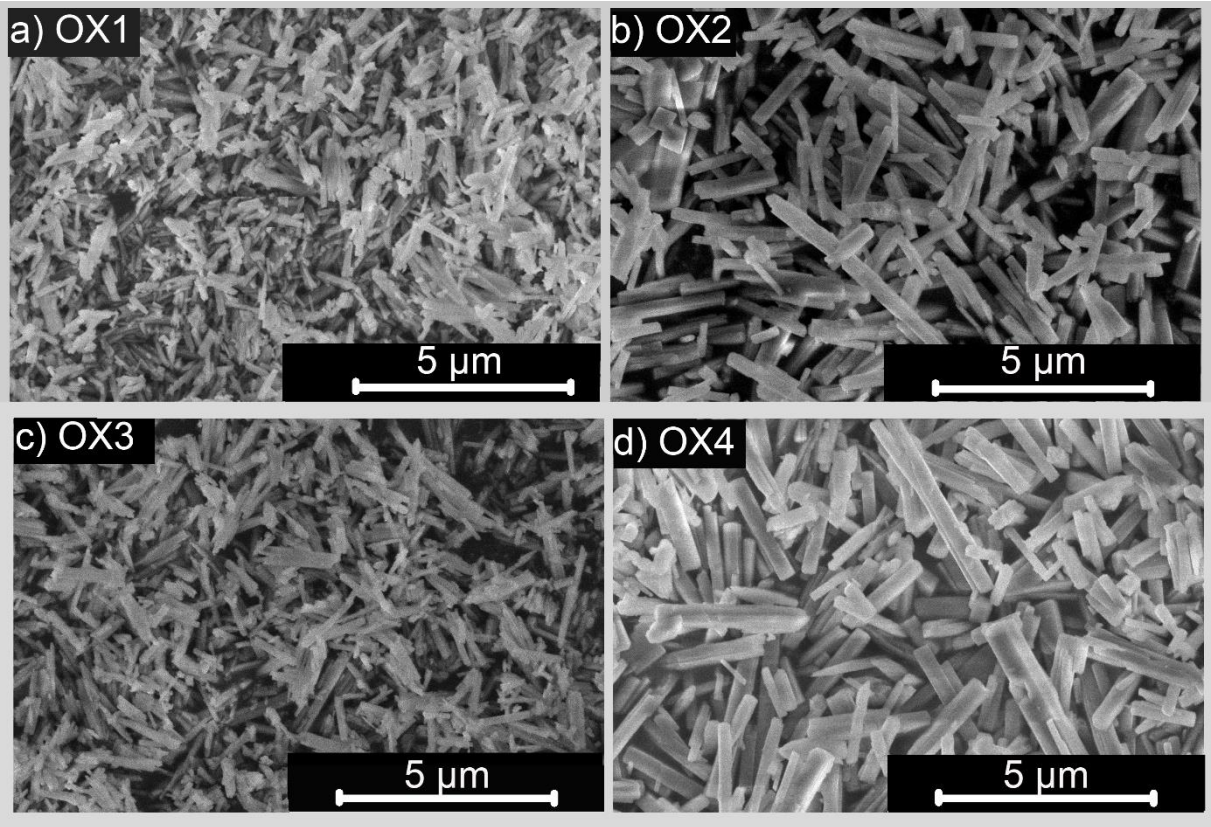

Figure 1: *SEM images of the OX1 (a), OX2 (b), OX3 (c) and OX4 (d) particles.*

As illustrated in the Figure 2, the diffraction peaks signify good crystallinity and can be indexed to the iron(II) oxalate dihydrate particles for all of the samples. According to Joint Committee on Powder Diffraction Standards (JCPDS), the iron(II) oxalate dihydrate card numbers 01-075-

7291 (lattice constants a = 12.26, b = 5.57, and c = 15.48) and 00-023-0293 (lattice constants a = 9.92, b = 5.55, and c = 9.70) for orthorhombic and monoclinic crystal system, respectively, were assigned. The most dominant diffraction peak (111) confirming the presence of the FeC_2O_4 phase, is located at approximately 21° of 2θ. Hence, the use of different synthesis conditions led to the iron(II) oxalate dihydrate particles in all cases. In the case of the OX3 sample, the additional diffraction peaks found at 11° and 31° of 2θ were attributed to orthorhombic Rhomboclase phase (JCPDS 00-080-6120). Rhomboclase is an acidic iron sulfate mineral with a formula $HFe(SO_4)_2 \cdot 4(H_2O)$ and its presence may be explained as a consequence of the iron(II) sulphate heptahydrate ($FeSO_4 \cdot 7H_2O$) reaction within the iron oxalate synthesis. It is considered that the stirring rate listed in Table 2 (100 or 500 rpm) has an influence on the crystal system.

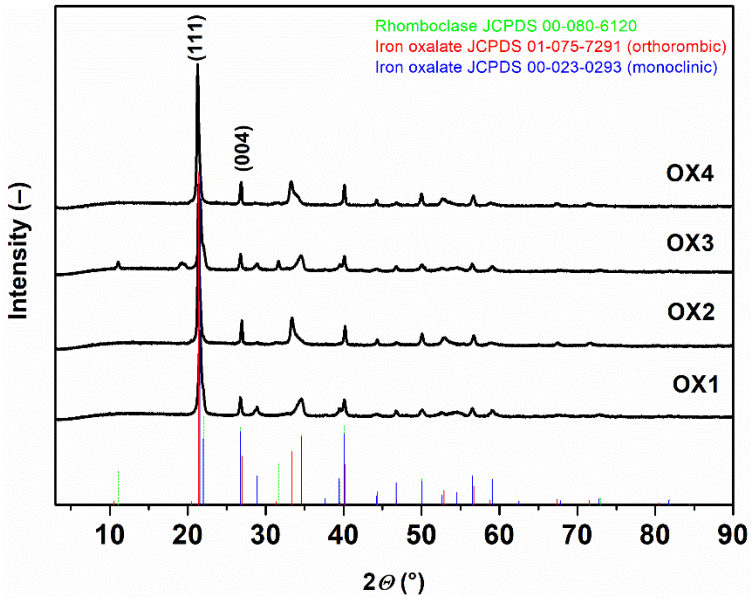

Figure 2: Powder XRD patterns of the iron(II) oxalate particles prepared under various synthesis conditions of OX1, OX2, OX3 and OX4.

As shown in Figure 2, the monoclinic crystal system is connected to OX1 and OX3 samples, whereas the orthorhombic system is present in case of OX2 and OX4 samples. The crystallite size of iron(II) oxalate particles was determined by the Scherrer's formula using the broadening

of (111) and (004) diffraction at about 21° and 26° of 2θ (Figure 2). The crystallite sizes are listed in the Table 3.

Table 3: Crystallite size (XRD), density and conductivity of the iron(II) oxalate particles under investigation.

Sample	**Crystallite size [nm]**	**Density [g·cm^{-3}]**	**Conductivity [S·m^{-1}]**
OX1	37	2.560 ± 0.003	5.1×10^{-7}
OX2	47	2.770 ± 0.016	8.2×10^{-12}
OX3	40	2.790 ± 0.007	4.4×10^{-8}
OX4	30	2.400 ± 0.047	4.9×10^{-12}

An optical microscope was used to study the behavior of the OX1 and the OX3 samples in the presence and the absence of an electric field. The particles exhibited random distribution in the absence of the electric field (Figs. 3a and 3c for OX1 and OX3, respectively). On the contrary, when an external electric field strength of 0.75 kV.mm^{-1} was applied (Fig. 3b and 3d for OX1 and OX3), the particles were assembled into highly organized internal chain-like structures between the electrodes. In addition, it was observed that OX3 particles formed more robust chain-like structures in comparison to OX1 particles, showing a better alignment overall. The stiffness of these internal structures is highly depended on the intensity of the electric field applied which will be quantified via a rheological analysis in the following section.

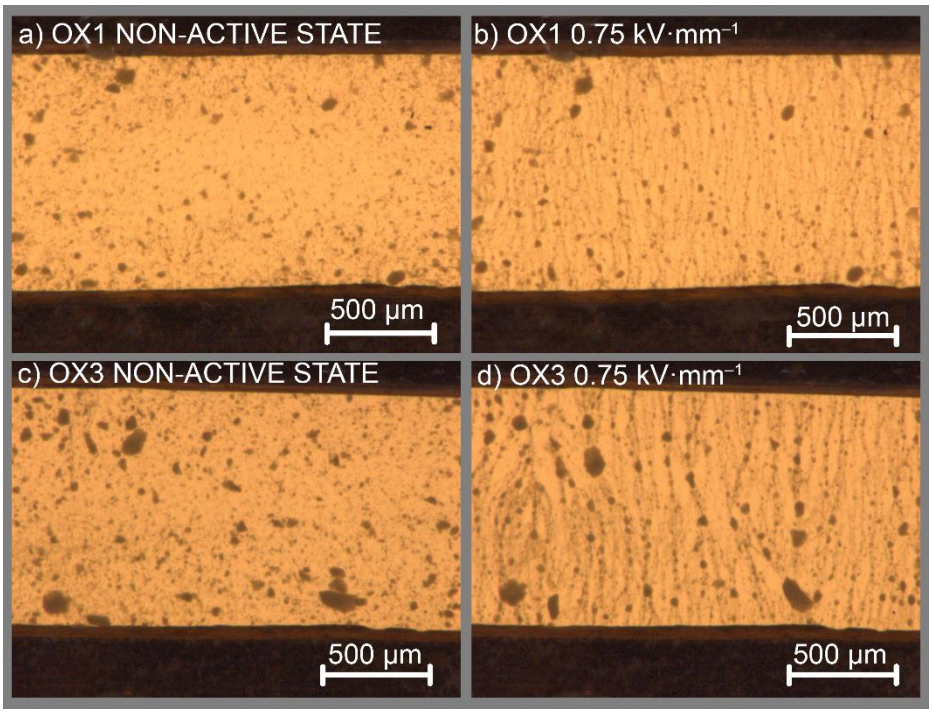

Figure 3: Optical microscopy images of the silicone oil suspensions containing iron(II) oxalate particles (0.5 vol%) synthesized under various synthesis conditions; Figures (a,b) and (c,d) correspond to samples OX1 and OX3, respectively. No electric field is applied on (a,c) while an external electric field strength of 0.75 kV·mm^{-1} is applied on (b,d).

Optical microscopy analysis was also used to study the longer OX2 and the OX4 particles with selected images shown in Fig. 4. Similarly to Fig. 3, without the presence of an electric field, these particles are randomly distributed throughout silicone oil.

In contrast, when an electric field is applied, these particles show a clear response which differs though from Fig. 3b,d. Both systems react on the electric field in an almost electrophoresis manner with chain-like structures between the electrodes rather close to the electrodes. To conclude the optical microscopy analysis, the ER behavior of the iron(II) oxalate particles is evidently affected by the synthesis conditions during the particles synthesis.

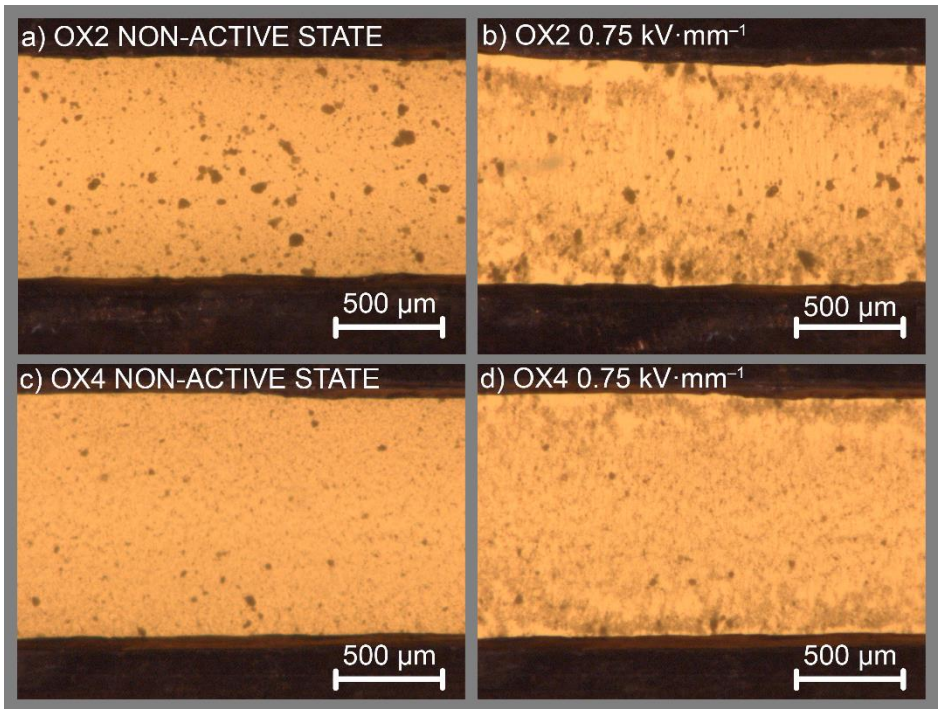

Figure 4: Optical microscopy images of the silicone oil suspensions containing the iron(II) oxalate particles (0.5 vol%) synthesized under various synthesis conditions; Figures (a,b) and (c,d) correspond to samples OX2 and OX4, respectively. No electric field is applied on (a,c) while an external electric field strength of 0.75 kV·mm^{-1} is applied on (b,d).

3.2. Electrorheological Behavior

The ER performance of the prepared ER suspensions based on the iron(II) oxalate particles synthesized under various synthesis conditions at a concentration of 5 vol% is shown in Fig. 5 (results for 10 vol% ER suspensions are shown in Fig. S2). It is apparent from Figure 5a, that all suspensions exhibit nearly Newtonian behavior in the absence of an external electric field [37], which is expressed as a linear increase in the shear stress in accordance with Newton's law:

$$\tau = \eta \cdot \dot{\boldsymbol{\gamma}} \qquad (2)$$

, where τ is the shear stress linearly proportional to the shear rate,$\dot{\boldsymbol{\gamma}}$, and η is the shear viscosity.

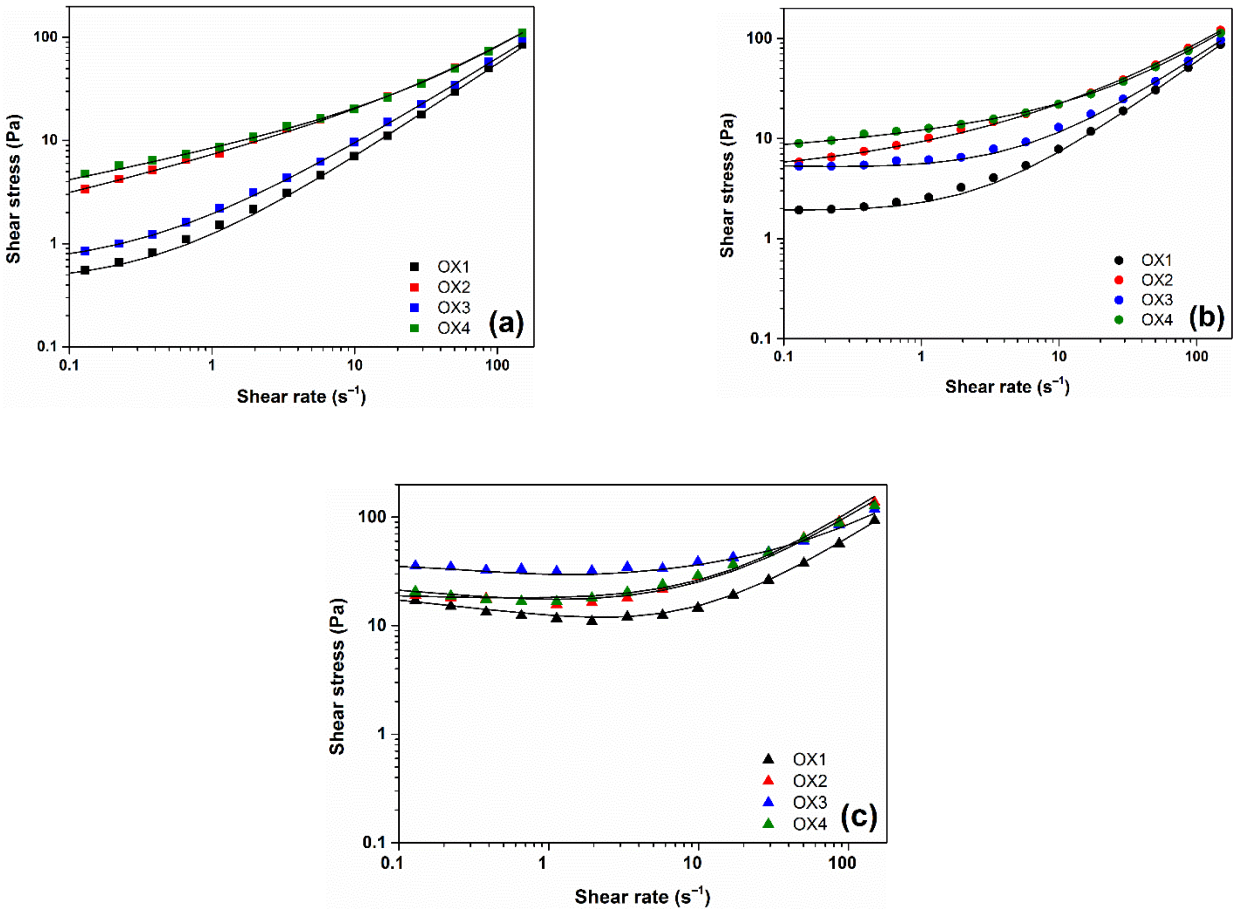

Figure 5: Shear stress as a function of shear rate for the ER suspensions containing the iron(II) oxalate particles prepared under various synthesis conditions (5 vol%) in the absence (a) and in the presence of electric field strengths of 0.3 kV·mm^{-1} (b) and 1.5 kV·mm^{-1} (c). The solid lines represent the CCJ model fit.

In the absence of electric field (Fig. 5a), stress, and consequently viscosity, follow the dimensional aspect of the rod-like particles (*L*) meaning that viscosity of the ER suspensions increases with increasing particle lengths, thus OX1 < OX3 < OX2 < OX4, as it is more difficult for the longer particles to orient along the direction of the flow. The effect of the external electric field is shown in Fig. 5b,c, where stress is enhanced when-the intensity of the electric field is increased. The suspensions begin to behave as pseudoplastic systems exhibiting a certain level of yield stress. To describe the phenomena taking place within the system macroscopically and the ER performance the following is generally applied. Once the electric

field is applied, the dispersed particles are polarized creating stiff and highly organized chain-like structures which are oriented along the direction of the electric field. These robust structures collapse only above a critical stress (yield stress), which is able to break down the chain-like structures allowing the material to flow due to the hydrodynamic forces. Further, yield stress is proportional to the electric field strength and disappears when the electric field is switched off.

For low electric fields the stress is generally increased (Fig. 5b), the lowest stress is observed for the OX1-based ER suspension followed by the OX3. Both systems were synthesized using the same stirring rate of 100 rpm. On the other hand, the ER suspensions based on the OX2 and the OX4 particles were synthesized at a higher stirring rate of 500 rpm and exhibit higher but very similar stress values at the corresponding shear conditions. Therefore, the length of the particle, thus the stirring rate during the synthesis of the iron(II) oxalate particles, appears to be a noteworthy aspect in their ER performance. It is apparent, that the OX1 and the OX3 samples, compared with the remaining two, show a lower ER effect which is attributed to their shorter length and agglomerates (Fig. 1). Interestingly, at higher electric fields (Fig. 5c), the flow curves of the OX1 sample aligns with the others namely OX2 and OX4 (probably due to the electrophoresis phenomena occurring in this samples at higher electric field strengths as illustrated in Fig. 4b,d not further increasing the stress with electric field), thus the stress values of these samples-based at the electric field of 1.5 $kV \cdot mm^{-1}$ do not differ. The observed stress values of the ER suspensions at low shear rates in Fig. 5 are approximately one order of magnitude higher when a sufficient electric field is applied. In particular, the OX3-suspension evidently possesses the highest stress values (Fig. 5c) under the same flow conditions. This is most probably a consequence of the highest aspect ratio of the OX3 particles fully manifesting the geometric benefit at higher electric fields, as it was proven that the aspect ratio plays a significant role in particles polarization and their interconnection into a stiffer internal chain-

like structure [27, 38]. In addition, as aforementioned in the optical microscopy analysis in Figs. 3 and 4, the OX3 particles create more robust chain-like structures in comparison with the others under investigation, contributing to a higher ER activity.

The ER performance can be quantitatively expressed using various models which can be fitted in Fig. 5 and from the fitting parameters relevant information such as yield stress can be extrapolated. The Cho-Choi-Jhon (CCJ) model is well-known as one of the most suitable rheological equation to describe the flow curves extracted from ER suspensions [39, 40]. Consequently, the CCJ model was used in this study to fit the flow curves to investigate the effect of morphology, thus, the synthesis conditions on the ER performance. The CCJ model contains six parameters (Eq. 3) describing the complex behavior of ER suspensions and fits well on the data throughout the entire shear rate regime. The CCJ model is described by the following equation [41]:

$$\tau = \frac{\tau_y}{1+(t_1\dot{\gamma})^{\alpha}} + \eta_{\infty} \cdot \left(1 + \frac{1}{(t_2\dot{\gamma})^{\beta}}\right) \cdot \dot{\gamma} \qquad (3)$$

, where τ_y is the dynamic yield stress, t_1 and t_2 are time constants describing the variation in shear stress. The exponent α is describing the decrease in the shear stress at low shear rates and the exponent β is takes values between 0–1, since $d\tau/d\dot{\gamma} > 0$, and η_{∞} represents the shear viscosity at high shear rates. The CCJ data fit is represented in Figure 5 with solid lines, with the parameters summarized in Tables 4 and 5.

One of the most important parameters obtained from the CCJ model is yield stress. As mentioned before the yield stress is enhanced when the electric field is applied with exact values shown in Tables 4 and 5. At low electric fields the sample which were prepared with a stirring rate of 500 rpm (OX2 and OX4) show a slightly higher yield stress although the picture changes at higher electric fields. As mentioned above, the OX2 and the OX4 particles possess a higher one-dimensional (L/D) character; therefore, leading to much stronger dipole-dipole interactions

between them. At higher electric fields all samples with the exception of OX3 share similar yield stress ~20 Pa, while the remaining suspension shows almost two times higher yield stress.

Table 4: Obtained CCJ model parameters for the ER suspension containing the iron(II) oxalate particles (5 vol%) synthesized with a stirring rate of 100 rpm for different electric field strengths.

	OX1			OX3		
	Electric field strength [kV·mm^{-1}]					
Parameters	**0**	**0.3**	**1.5**	**0**	**0.3**	**1.5**
τ_y	0.5	1.9	19.2	0.7	4.5	37.4
t_1	0.72	1.34	9.68	0.32	2.45	3.06
α	0.01	0.10	0.31	0.01	0.09	0.90
η_∞	0.24	0.29	0.37	0.24	0.31	0.42
t_2	0.01	0.01	0.03	0.01	0.01	0.01
β	0.14	0.02	0.31	0.23	0.13	0.86

Table 5: Obtained CCJ model parameters for the ER suspension containing the iron(II) oxalate particles (5 vol%) synthesized with a stirring rate of 500 rpm for different electric field strengths.

	OX2			OX4		
	Electric field strength [kV·mm^{-1}]					
Parameters	**0**	**0.3**	**1.5**	**0**	**0.3**	**1.5**
τ_y	2.8	5.7	21.3	4.0	7.8	23.1
t_1	0.35	2.74	6.02	0.37	2.42	7.92
α	0.12	0.09	0.10	0.09	0.08	0.40

η_∞	0.46	0.48	0.84	0.50	0.57	0.75
t_2	0.01	0.01	0.94	0.02	0.03	0.05
β	0.63	0.57	0.39	0.70	0.77	0.70

There are two methods to evaluate the ER performance of these systems for their potential application. The first is based on reaching as high yield stress as possible when an external electric field is applied while the second is related to the relative change of the system's stiffness caused by the presence of the electric field. The later can be expressed in terms of the ER efficiency, defined as the relative change of viscosity of the ER suspension in its on-state and off-state and shown by the following equation:

$$e = \frac{\eta_E - \eta_0}{\eta_0} \quad (4)$$

, where η_E and η_0 is a viscosity in the presence and absence of the electric field, respectively.

As can be seen in Fig. 6, higher electric fields show a superior efficiency as a consequence of higher particles polarization while the synthesis conditions seems to not affect the efficiency.

The efficiency is increasing in the following sequence: OX2 < OX4 < OX1 < OX3. Similarly to the other parameters, the dependance of the efficiency is related to the particle's morphology and aspect ratio, thus its synthesis conditions. Particles with shorter dimensions show a lower viscosity which results in high efficiencies (Eq. (4)). To conclude, the stirring rate during the synthesis of the particles has a distinct influence on efficiency.

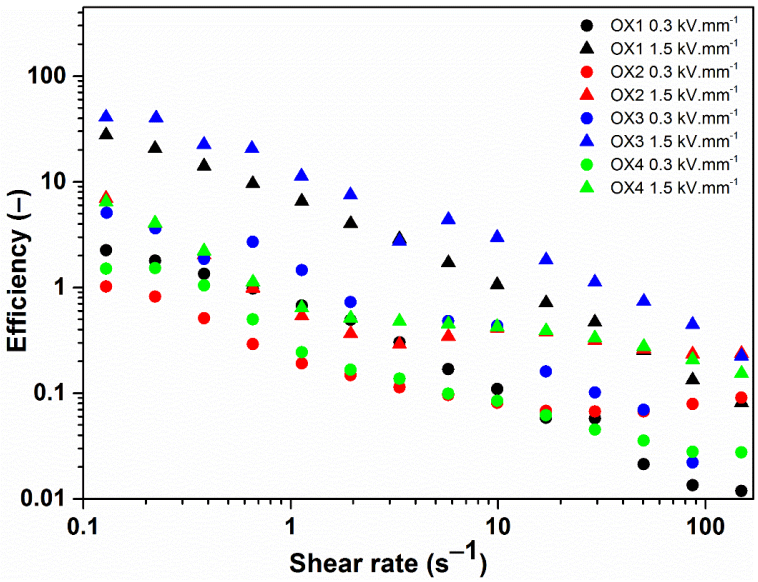

Figure 6: Dependences of the ER efficiency on the shear rate for the ER systems consisted of the iron(II) oxalate particles (5 vol%) synthesized under various synthesis conditions exposed to the external electric field of the strength 0.3 kV.mm^{-1} (circles) and 1.5 kV.mm^{-1} (triangles).

Increasing the sedimentation stability of ER fluids is very important for their applications. Poor sedimentation stability is still a considerable problem in the current ER suspensions. The highest sedimentation ratio obtained from a visual observation of the separating phase boundaries as a function of time was observed for the sample OX3 (Fig. 7), which also possesses the highest ER effect (Fig. 5c) and efficiency (Fig. 6) due to its morphology.

Sedimentation stability in terms of the sedimentation ratio was 0.9 after 60 hours at rest which is a promising result in comparison with the ER systems of similar particles concentrations [42]. From the application point of view, any ER fluid with sedimentation ration above 0.9 is considered to have excellent stability.

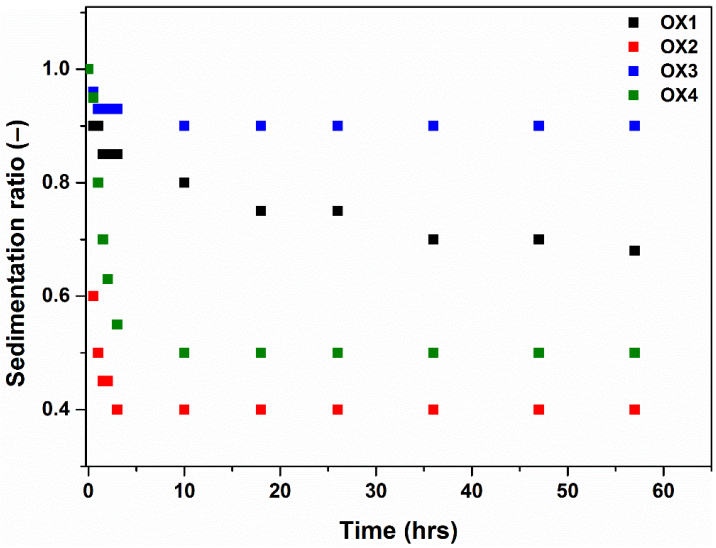

Figure 7: Sedimentation stability as a function of time for the ER suspensions based on the iron(II) oxalate particles (5 vol%) synthesized under various synthesis conditions dispersed in a silicone oil.

4. Conclusion

The present study describes the successful synthesis of the iron(II)oxalate particles which were prepared by a co-precipitation method using iron(II) sulphate heptahydrate and oxalic acid dihydrate as precursors. In particular, the research was focused on the preparation of particles with different dimensions. The preparation was performed under various synthesis conditions, mainly the drip and stirring rate. Selected particles possessing a rod-like shape with different lengths and diameters were further examined using an X-ray diffraction analysis to confirm the presence of the dominant FeC_2O_4 phase. It was found that faster stirring rates resulted in more robust particles and had an influence on their crystallite size. Subsequently, the prepared particles were used as a dispersed phase in the ER suspensions at the concentration of 5 vol%. The ER suspension based on the OX3 particles exhibited the highest yield stress under external electric field strength of 1.5 $kV \cdot mm^{-1}$ which was almost two times higher in comparison with the other samples. It was found that a high aspect ratio of the particles plays a significant role

as far as the ER behavior is concerned. Similarly to yield stress, the highest ER efficiency was observed for the system consisting of the OX3 particles. Finally, the highest sedimentation stability of the prepared particles in a silicone oil was proven for the OX3 sample, probably due to its geometrical parameters which make the attractions entropically unfavored. It was experimentally proven that the synthesis conditions have a significant impact on the final shape and structure of particles reflecting in their overall ER performance.

Acknowledgment

The authors wish to thank the Internal Grant Agency of Tomas Bata University in Zlín (projects nos. IGA/CPS/2019/005) for its financial support. The authors E.K., A.R., D.S. and M.S. gratefully acknowledge project DKRVO (RP/CPS/2020/006) supported by the Ministry of Education, Youth and Sports of the Czech Republic.

References

[1] Kutalkova E, Plachy T, Sedlacik M. On the enhanced sedimentation stability and electrorheological performance of intelligent fluids based on sepiolite particles. J Mol Liq. 2020;309:7.

[2] Yin JB, Wang XX, Chang RT, Zhao XP. Polyaniline decorated graphene sheet suspension with enhanced electrorheology. Soft Matter. 2012;8(2):294-7.

[3] Xi ZY, Ma JB, Sun WJ, Wang BX, Hao CC. Synthesis and electrorheological properties of hierarchical and core-shell MoS2@TiO2 nanocomposite. J Solid State Chem. 2020;290:12.

[4] Wereley NM, Lindler J, Rosenfeld N, Choi YT. Biviscous damping behavior in electrorheological shock absorbers. Smart Mater Struct. 2004;13(4):743-52.

[5] Nikitczuk J, Weinberg B, Canavan PK, Mavroidis C. Active Knee Rehabilitation Orthotic Device With Variable Damping Characteristics Implemented via an Electrorheological Fluid. IEEE-ASME Trans Mechatron. 2010;15(6):952-60.

[6] Mazursky A, Koo JH, Yang TH. Design, modeling, and evaluation of a slim haptic actuator based on electrorheological fluid. J Intell Mater Syst Struct. 2019;30(17):2521-33.

[7] Tonazzini A, Sadeghi A, Mazzolai B. Electrorheological Valves for Flexible Fluidic Actuators. Soft Robotics. 2016;3(1):34-41.

[8] Behbahani SB, Tan XB. Design and dynamic modeling of electrorheological fluid-based variable-stiffness fin for robotic fish. Smart Materials and Structures. 2017;26(8).

[9] Liu YJ, Davidson R, Taylor P. Touch sensitive electrorheological fluid based tactile display. Smart Mater Struct. 2005;14(6):1563-8.

[10] Liu YD, Lee BM, Park TS, Kim JE, Choi HJ, Booh SW. Optically transparent electrorheological fluid with urea-modified silica nanoparticles and its haptic display application. J Colloid Interface Sci. 2013;404:56-61.

[11] Biswas S, Visell Y. Emerging Material Technologies for Haptics. Adv Mater Technol. 2019;4(4):30.

[12] Liu YD, Choi HJ. Electrorheological fluids: smart soft matter and characteristics. Soft Matter. 2012;8(48):11961-78.

[13] Davidson JR, Krebs HI. An Electrorheological Fluid Actuator for Rehabilitation Robotics. IEEE-ASME Trans Mechatron. 2018;23(5):2156-67.

[14] Jun CS, Kwon SH, Choi HJ, Seo Y. Polymeric Nanoparticle-Coated Pickering Emulsion-Synthesized Conducting Polyaniline Hybrid Particles and Their Electrorheological Study. ACS Appl Mater Interfaces. 2017;9(51):44811-9.

[15] Sun WJ, Ma JB, Xi ZY, Lin YS, Wang BX, Hao CC. Titanium oxide-coated titanium-loaded metal organic framework (MOF-Ti) nanoparticles show improved electrorheological performance. Soft Matter. 2020;16(40):9292-305.

[16] Zheng F. Thermophoresis of spherical and non-spherical particles: a review of theories and experiments. Adv Colloid Interface Sci. 2002;97(1-3):255-78.

[17] Yin JB, Xia XA, Xiang LQ, Zhao XP. Coaxial cable-like polyaniline@titania nanofibers: facile synthesis and low power electrorheological fluid application. J Mater Chem. 2010;20(34):7096-9.

[18] Abdelhalim MAK, Mady MM, Ghannam MM. Rheological and dielectric properties of different gold nanoparticle sizes. Lipids in Health and Disease. 2011;10.

[19] Plachy T, Sedlacik M, Pavlinek V, Stejskal J. The observation of a conductivity threshold on the electrorheological effect of p-phenylenediamine oxidized with p-benzoquinone. J Mater Chem C. 2015;3(38):9973-80.

[20] Dong YZ, Yin JB, Yuan JH, Zhao XP. Microwave-assisted synthesis and high-performance anhydrous electrorheological characteristic of monodisperse poly(ionic liquid) particles with different size of cation/anion parts. Polymer. 2016;97:408-17.

[21] Kim MH, Sae DH, Choi HJ, Seo Y. Synthesis of semiconducting poly(diphenylamine) particles and analysis of their electrorheological properties. Polymer. 2017;119:40-9.

[22] Wu JH, Jin T, Liu FH, Guo JJ, Cui P, Cheng YC, et al. Preparation of rod-like calcium titanyl oxalate with enhanced electrorheological activity and their morphological effect. J Mater Chem C. 2014;2(28):5629-35.

[23] Sedlacik M, Mrlik M, Kozakova Z, Pavlinek V, Kuritka I. Synthesis and electrorheology of rod-like titanium oxide particles prepared via microwave-assisted molten-salt method. Colloid Polym Sci. 2013;291(5):1105-11.

[24] Yoon CM, Noh J, Jang Y, Jang J. Fabrication of a silica/titania hollow nanorod and its electroresponsive activity. RSC Adv. 2017;7(32):19754-63.

[25] Mrlik M, Pavlinek V, Saha P, Quadrat O. Electrorheological properties of suspensions of polypyrrole-coated titanate nanorods. Appl Rheol. 2011;21(5):7.

[26] Erol O, Unal HI. Core/shell-structured, covalently bonded TiO2/poly(3,4-ethylenedioxythiophene) dispersions and their electrorheological response: the effect of anisotropy. RSC Adv. 2015;5(125):103159-71.

[27] Noh J, Yoon CM, Jang J. Enhanced electrorheological activity of polyaniline coated mesoporous silica with high aspect ratio. J Colloid Interface Sci. 2016;470:237-44.

[28] Vincenzi D. Orientation of non-spherical particles in an axisymmetric random flow. J Fluid Mech. 2013;719:465-87.

[29] Yin JB, Zhao XP. Electrorheological properties of titanate nanotube suspensions. Colloid Surf A-Physicochem Eng Asp. 2008;329(3):153-60.

[30] Pei J, Chen G, Li X, Li YX, Zhou N. Molten salt synthesis and thermoelectric properties of Ca2Co2O5. Mater Lett. 2009;63(17):1459-61.

[31] Cai ZY, Xing XR, Li L, Xu YM. Molten salt synthesis of lead lanthanum zirconate titanate ceramic powders. J Alloy Compd. 2008;454(1-2):466-70.

[32] Zhao SX, Li Q, Wang L, Zhang YL. Molten salt synthesis of lead lanthanum zirconate titanate stannate powders and ceramics. Mater Lett. 2006;60(3):425-30.

[33] Nidhin M, Indumathy R, Sreeram KJ, Nair BU. Synthesis of iron oxide nanoparticles of narrow size distribution on polysaccharide templates. Bull Mat Sci. 2008;31(1):93-6.

[34] Mahdavi M, Bin Ahmad M, Haron MJ, Namvar F, Nadi B, Ab Rahman MZ, et al. Synthesis, Surface Modification and Characterisation of Biocompatible Magnetic Iron Oxide Nanoparticles for Biomedical Applications. Molecules. 2013;18(7):7533-48.

[35] Dong YZ, Esmaeilnezhad E, Choi HJ. Core-Shell Structured Magnetite-Poly(diphenylamine) Microspheres and Their Tunable Dual Response under Magnetic and Electric Fields. Langmuir. 2021;37(7):2298-311.

[36] Plachy T, Cvek M, Kozakova Z, Sedlacik M, Moucka R. The enhanced MR performance of dimorphic MR suspensions containing either magnetic rods or their non-magnetic analogs. Smart Mater Struct. 2017;26(2):8.

[37] Hao T. Electrorheological suspensions. Adv Colloid Interface Sci. 2002;97(1-3):1-35.

[38] Yoon CM, Lee K, Noh J, Lee S, Jang J. Electrorheological performance of multigram-scale mesoporous silica particles with different aspect ratios. J Mater Chem C. 2016;4(8):1713-9.

[39] Choi K, Nam JD, Kwon SH, Choi HJ, Islam MS, Kao N. Microfibrillated Cellulose Suspension and Its Electrorheology. Polymers. 2019;11(12):11.

[40] Park IH, Kwon SH, Choi HJ. Emulsion-polymerized polyindole nanoparticles and their electrorheology. J Appl Polym Sci. 2018;135(25):9.

[41] Liu J, Wen XH, Liu ZP, Tan Y, Yang SY, Zhang P. Electrorheological performances of poly(o-toluidine) and p-toluenesulfonic acid doped poly(o-toluidine) suspensions. Colloid Polym Sci. 2015;293(5):1391-400.

[42] Mrlik M, Ilcikova M, Osicka J, Kutalkova E, Minarik A, Vesel A, et al. Electrorheology of SI-ATRP-modified graphene oxide particles with poly(butyl methacrylate): effect of reduction and compatibility with silicone oil. RSC Adv. 2019;9(3):1187-98.